[4] Ignagni, M. B. (1990)
Separate-bias Kalman estimator with bias state noise.
IEEE Transactions on Automatic Control, **33**, 3 (1990), 338–341.

[5] Hsieh, C.-S., and Chen, F.-C. (1999)
Optimal solution of the two-stage Kalman estimator.
IEEE Transactions on Automatic Control, **44**, 1 (1999), 194–199.

[6] Ignagni, M. B. (2000)
Optimal and suboptimal separate-bias Kalman estimators for a stochastic bias.
IEEE Transactions on Automatic Control, **45**, 3 (2000), 547–551.

[7] Heffes, H. (1966)
The effect of erroneous models on the Kalman filter response models.
IEEE Transactions on Automatic Control, **11** (1966), 541–543.

[8] Fitzgerald, R. J. (1971)
Divergence of the Kalman filter.
IEEE Transactions on Automatic Control, **AC-16** (1971), 736–747.

[9] Kwon, W. H., Kim, P. S., and Park, P. (1999)
A receding horizon Kalman FIR filter for discrete time-invariant systems.
IEEE Transactions on Automatic Control, **44**, 9 (1999), 1787–1791.

[10] Kwon, W. H., Kim, P. S., and Han, S. H.
A receding horizon unbiased FIR filter for discrete-time state space models.
Automatica, **38**, 3 (2002), 545–551.

[11] Jiang, H., Yang, W.-Q., and Yang, Y.-T. (1996)
State space modeling of random drift rate in high-precision gyro.
IEEE Transactions on Aerospace and Electronic Systems, **32**, 3 (1996), 1138–1143.

Innovative Estimation Method with Measurement Likelihood for All-Accelerometer Type Inertial Navigation System

This work presents an innovative estimation scheme to solve the initial and divergent problems for an all-accelerometer inertial navigation system (INS). The proposed system uses six accelerometers mounted diagonally on each surface of a cubic. The system proposed herein exploits additional information involving the gravity effect, allowing us to determine the angular velocity. It also provides an upper bound value to initiate the platform attitude. In addition, an estimation algorithm using the own-ship trajectory estimator providing a *measurement likelihood* is proposed. A simulation case for estimating position and velocity of the vehicle is investigated by this approach. Results confirm the effectiveness of this information infusing concept in obtaining a convergent INS state estimation.

Manuscript received March 9, 1998; revised June 21, 2001; released for publication December 3, 2001.

IEEE Log No. T-AES/38/1/02601.

Refereeing of this contribution was handled by X. R. Li.

This research was supported by National Science Council Grant (NSC 89-2212-E-014-026) of Republic of China.

I. INTRODUCTION

The conventional inertial navigation system (INS) uses linear accelerometers to sense linear acceleration, as well as uses gyroscopes to measure angular velocity or angular position. Ground alignment or prelaunch alignment of inertial platform has received extensive interest in the design of an inertial navigation system. The gyrocompassing technique, a conventional mode of alignment and calibration, has been applied to this problem for quite some time. This techniques finds the derivation angle between the inertial platform and local gravity vector, i.e., leveling, and seeks the true north by sensing the rotation of the Earth just as the gyrocompassing does [1]. The kinematics of a rigid body can also be determined by using only linear accelerometers. This topic has received extensive attention from diverse disciplines such as inertial navigation, experimental modal analysis, and biomechanical research. In theory, a minimum of six linear accelerometers are necessary [2–6]. Among the numerous attempts to mechanize a minimum accelerometer configuration, a nine accelerometer configuration was developed to yield a stable solution. Chen, et al. in 1994 [7] also presented a novel scheme using only six accelerometers.

Chen's investigation demonstrated the effectiveness of a workable scheme for a gyroscope free strapdown inertial measurement unit by using only six linear accelerometers. The six accelerometer measurements are combined to compute the rotational and translational accelerations of a rigid body. Resolving this problem hinges on selecting the location and orientation of these accelerometers. The design places the accelerometer at the surface center of a cube, with the sensing axis of each accelerometer aligned diagonally along the respective cube surface. The linear and rotational accelerations are combined from the six accelerometer measurements. Integrating angular acceleration with given initial condition yields the angular velocity. Notably, the configuration computes translation acceleration of the center of gravity (CG) from the accelerometer measurements as well as the knowledge of angular velocity ω, which appears as ω^2 term in the state equation. However, the configuration is limited in that angular velocity ω cannot be determined by linear accelerometers. Chen's investigation evaded this issue by measuring only the angular acceleration and computing the angular velocity as the time integral of angular acceleration. If the initial value is not zero, some means must be derived to measure it.

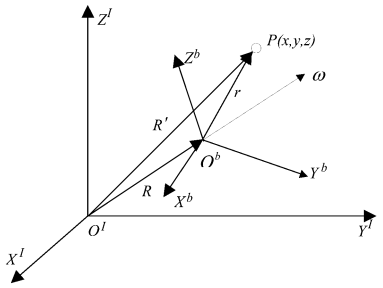

Fig. 1. Geometry of inertial frame (I) and body frame (b).

The estimation error equation characteristic equation (EEECE) [8] addresses the problem of providing the initial value and the correct sign for $\omega(0)$. A constraint exists for the EEECE, i.e., it does not have $s = 0$ roots when linearized around a nonlinear nominal angular velocity (ω_{ref}). In our approach, the estimation process is in standard form with the computed CG acceleration considered as states and the sensor measurement as a control. In such a form, no measurements are provided. The stability of the estimation process, i.e., the EEECE, is independent of estimation gains. In addition, the stability is enhanced with the presence of gravity (G) in the accelerometers, thereby limiting the initial attitude (θ) and, to some extent, providing a bound for the ω sign problem.

In light of the above developments, this work presents a novel method of resolving the initial value problem for ω in a planar problem (θ, x, y). The angular velocity ω can be estimated on line within the estimation process through the state propagation of initial attitude as obtained from the gravity probe by applying the Kalman filtering technique. It has the $G(\theta)$ part but not the ω^2 part.

This work also proposes an innovative estimation method to solve the initial and divergent problems for an all-accelerometer INS with a recursive least squares format [9], called the Own-Ship Trajectory Estimator (OTE). In doing so, a current input vector of the conventional Kalman filter (CKF) can be generated. The OTE method uses the processed data, *measurement likelihood* [10–13] which is created from OTE, and the output of the CKF at a previous time step, to estimate the values of the position and velocity, which are then fed to the CKF to correct the system outputs. Moreover a combined scheme of this trajectory estimator and the CKF significantly upgrades the navigational accuracy of six-accelerometer type INS.

II. DYNAMIC DESCRIPTION

Two coordinates systems, the inertial frame (O^I, X^I, Y^I, Z^I) and the rotational moving body frame (O^b, X^b, Y^b, Z^b), are considered in the motion of a vehicular system as shown in Fig. 1. The acceleration at point P is given by [13, 14]

$$\mathbf{a} = \ddot{\mathbf{R}}_I + \ddot{\mathbf{r}}_\mathbf{b} + \dot{\omega} \times \mathbf{r} + 2\omega \times \dot{\mathbf{r}}_b + \omega \times (\omega \times \mathbf{r}) \quad (1)$$

where

ω inertial angular velocity of body frame,
$\ddot{\mathbf{r}}_\mathbf{b}$ acceleration of point P relative to body frame,
$\ddot{\mathbf{R}}_I$ inertial acceleration of CG at O^b relative to O^I,
$\dot{\omega} \times \mathbf{r}$ tangential acceleration owing to angular acceleration of rotating frame,
$\omega \times (\omega \times \mathbf{r})$ centripetal acceleration,
$2\omega \times \dot{\mathbf{r}}_b$ Coriolis acceleration.

The terms $\dot{\mathbf{r}}_\mathbf{b}$ and $\ddot{\mathbf{r}}_\mathbf{b}$ in (1) vanish since P is fixed on the body frame. The accelerometer is a precision instrument designed to measure a component of the vector quantity called specific force **f**. It is defined by

$$\mathbf{f} = \mathbf{a} - \mathbf{g}$$

where **a** is inertial acceleration and **g** is gravitational attraction per unit mass. In navigation computation, we must calculate **g** and use $\mathbf{f} + \mathbf{g}$ to obtain the inertial acceleration **a** of a moving vehicle. For simplicity and without loss of generality, we neglect the gravitation effect in the following discusion.

Measurement of the ith accelerometer in a six-accelerometer scheme at offset point $\mathbf{r}_i$ yields

$$\begin{aligned} A_i &= \mathbf{a} \cdot \alpha_i \\ &= [\ddot{\mathbf{R}}_I + \dot{\Omega}\mathbf{r}_i + \Omega\Omega\mathbf{r}_i] \cdot \alpha_i, \qquad i = 1, 2, \ldots, 6 \end{aligned} \quad (2)$$

where α_i represents the unit vector along sensing orientation and Ω is a skew-symmetric matrix of angular velocity.

Equation (2) expresses a combination of the linear acceleration $\ddot{\mathbf{R}}$, tangential acceleration $\dot{\Omega}\mathbf{r}$, and centripetal acceleration $\Omega\Omega\mathbf{r}$. We wish to substract the rotational terms from the sensed acceleration A_i in order to obtain the linear acceleration at CG.

A configuration description and mechanization equation for six-accelerometer design was presented by Chen, et al. in which the rotational acceleration $\dot{\omega}$ is obtained from a linear combination of the accelerometer output, but the translational CG acceleration is computed from the sensor measurements as well as the knowledge of the angular velocity ω as follows

$$\begin{bmatrix} \dot{\omega} \\ \cdots \\ (\ddot{\mathbf{R}})_I \end{bmatrix} = \frac{1}{2} \begin{bmatrix} \frac{1}{\rho}\mathbf{S} \\ \cdots \\ \mathbf{T} \end{bmatrix} \begin{bmatrix} A_{1o} \\ A_{2o} \\ A_{3o} \\ A_{4o} \\ A_{5o} \\ A_{6o} \end{bmatrix} + \rho \begin{bmatrix} 0 \\ 0 \\ 0 \\ \omega_y\omega_z \\ \omega_x\omega_z \\ \omega_x\omega_y \end{bmatrix} \quad (3)$$

where **S** and **T** denote the location and orientation matrices, respectively [7], ρ is a dimensionless unit

length, and subscript o means for the sensor's output. The ω appears as ω^2 term in the state equation. The problem of providing the initial value and the correct sign for $\omega(0)$ are addressed by the EEECE. There is a constraint for EEECE, that it should have no zero root, see Appendix A.

For the consideration of navigation used, we write the dynamic equation for the six-accelerometer configuration. If we rearrange the sensing direction of accelerometers, see Appendix B, the gravity may play an important role to indicate the attitude of vehicle θ. It has the states position $\mathbf{p}$ (as a vector), velocity $\mathbf{V}$, and acceleration $\mathbf{a}$, orientation θ (generic name), angular velocity ω as well as angular acceleration $\dot{\omega}$. The equation of motion can be written as

$$\dot{\mathbf{p}} = \mathbf{V} \tag{4}$$

$$\dot{\mathbf{V}} = \frac{\mathbf{F}}{m} + \frac{\mathbf{dist}_1}{m} + \mathbf{g} \tag{5}$$

$$\dot{\theta} = \omega \tag{6}$$

$$\dot{\omega} = \mathbf{I}^{-1}(-\omega \times \mathbf{I} \cdot \omega + \mathbf{M} + \mathbf{dist}_2). \tag{7}$$

In (4)–(7), $\mathbf{F}$ is a known and controllable force, $\mathbf{M}$ is a known moment and could be treated as a control, $\mathbf{g}$ denotes the gravity, and $\mathbf{dist}_i$, $i = 1, 2$, means the disturbance, and m expresses the mass, and $\mathbf{I}$ is moment of inertia. Our sensor measurements are the six-accelerometer output. The measurement parameters are

$$Y = Y(\dot{\mathbf{V}}, \dot{\omega}, G(\theta)). \tag{8}$$

By grouping, we can also make this into two specific sets of measurement

$$y_{\dot{\omega}} = y_{\dot{\omega}}(\dot{\omega}) \tag{9}$$

$$y_a = y_a(\dot{\mathbf{V}}, G(\theta)). \tag{10}$$

Using (54) and (9)–(10), we can rewrite (4)–(7), which become no additional measurement equation (the measurement of accelerometer as a control input), it are

$$\dot{\mathbf{p}} = \mathbf{V} \tag{11}$$

$$\dot{\mathbf{V}} = y_a(\mathbf{V}, G(\theta)) - \gamma_a \tag{12}$$

$$\dot{\theta} = \omega \tag{13}$$

$$\dot{\omega} = y_{\dot{\omega}}(\dot{\omega}) - \gamma_\omega \tag{14}$$

where γ_a and $\gamma_{\dot{\omega}}$ are both accelerometer bias that can be treated as a statistic quantities, and $G(\theta)$ plays the role just like a spring in a mass-spring motion. Since there are limits to velocity in a realistic mission and the sense of $\dot{\omega}$ will result in the change of θ, it will reflect the value of G in horizontal direction, especially when it exceeds a reasonable bounded value.

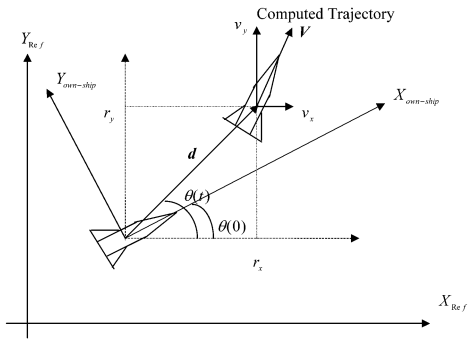

Fig. 2. Own-ship geometry.

III. NOVEL ESTIMATION EQUATION

Equations (11)–(14) had turned the highest derivative measurement into a control term in the state dynamic equation. Therefore, a problem arises that there is no measurement equation. Any additional measurements $\mathbf{p}, \mathbf{V}, \theta, \omega$ will help to construct the estimation processing. A novel estimation scheme associated with the CKF for an unobservable system is introduced in this section.

Consider the geometry depicted in Fig. 2 that the reference frame and own-ship are confined to the same plane. Define states vector for the planar motion as

$$\mathbf{D} = [\,x(t) \quad y(t) \quad v_x(t) \quad v_y(t) \quad \theta(t) \quad \omega(t)\,]^T. \tag{15}$$

The states equations are then

$$\dot{x} = v_x \tag{16a}$$

$$\dot{y} = v_y \tag{16b}$$

$$\dot{v}_x = y_{ax}\cos\theta - y_{ay}\sin\theta \tag{16c}$$

$$\dot{v}_y = y_{ax}\sin\theta + y_{ay}\cos\theta \tag{16d}$$

$$\dot{\theta} = \omega \tag{16e}$$

$$\dot{\omega} = y_{\dot{\omega}} \tag{16f}$$

where (see Appendix B)

$$y_{ax} = \frac{A_{o1} - A_{o3}}{2} + \delta a_x \tag{17}$$

$$y_{ay} = -\frac{(A_{o2} - A_{o4})}{2} + \delta a_y \tag{18}$$

$$y_{\dot{\omega}} = \frac{A_{o1} + A_{o2} + A_{o3} + A_{o4}}{4} + \delta\dot{\omega} \tag{19}$$

and δa_x, δa_y, and $\delta\dot{\omega}$ mean the measurement noises of sensor. The measurement is the gravity sensing from a static initial condition that provides a Euler angle of the vehicular with respect to the inertial frame. The system dynamic equations in matrix form become

$$\dot{\mathbf{D}} = \mathbf{FD} + \mathbf{Gu} + \Gamma\,\mathbf{W} \tag{20}$$

$$E = \mathbf{HD} + \varepsilon \tag{21}$$

where ε and $\mathbf{W}$ denote the measurement noise matrix and the system process noise matrix respectively, and

$$\mathbf{F}=\begin{bmatrix}0&0&1&0&0&0\\0&0&0&1&0&0\\0&0&0&0&0&0\\0&0&0&0&0&0\\0&0&0&0&0&1\\0&0&0&0&0&0\end{bmatrix}\qquad \mathbf{G}=\begin{bmatrix}0&0&0\\0&0&0\\\cos\theta&-\sin\theta&0\\\sin\theta&\cos\theta&0\\0&0&0\\0&0&1\end{bmatrix}$$

$$\Gamma=\begin{bmatrix}0&0&0\\0&0&0\\\cos\theta&-\sin\theta&0\\\sin\theta&\cos\theta&0\\0&0&0\\0&0&1\end{bmatrix}\qquad \mathbf{H}=[0\quad 0\quad 0\quad 0\quad 1\quad 0]$$

$$\mathbf{u}=\begin{bmatrix}\dfrac{A_{o1}-A_{o3}}{2}\\-\dfrac{(A_{o2}-A_{o4})}{2}\\\dfrac{A_{o1}+A_{o2}+A_{o3}+A_{o4}}{4}\end{bmatrix}\qquad \mathbf{W}=\begin{bmatrix}\delta a_x\\\delta a_y\\\delta a_z\end{bmatrix}.$$

The equations for the own-ship trajectory can be obtained by referring to the geometry configuration depicted in Fig. 2. Then we have

$$d(t)=\|\mathbf{d}(t)\|=\sqrt{d_x^2+d_y^2} \tag{22}$$

$$\theta(t)=\tan^{-1}\left(\frac{d_y}{d_x}\right) \tag{23}$$

where $\mathbf{d}(t)$ is the instantaneous own-ship position in reference frame, $\theta(t)$ stands for the Euler angle defined as between own-ship position and reference coordinate, and

$$d_x=d\cos\theta \tag{24}$$

$$d_y=d\sin\theta. \tag{25}$$

Thus, the velocity of own-ship in reference frame can be represented as

$$v=\sqrt{v_x^2+v_y^2} \tag{26}$$

where

$$v_x=\dot{d}\cos\theta-d\dot{\theta}\sin\theta=x_3 \tag{27}$$

$$v_y=\dot{d}\sin\theta+d\dot{\theta}\cos\theta=x_4. \tag{28}$$

From (24) and (25), we have

$$\dot{d}=\frac{d_x\dot{d}_x+d_y\dot{d}_y}{\sqrt{d_x^2+d_y^2}}. \tag{29}$$

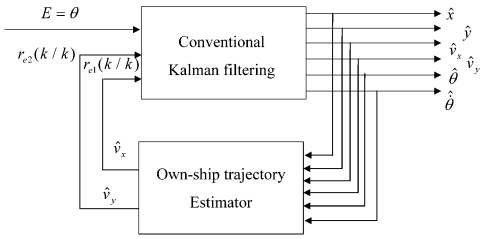

Fig. 3. Scheme of measurement likelihood.

The own-ship trajectory dynamics can be rewritten in terms of states as

$$\dot{x}_1=\frac{x_1x_3+x_2x_4}{\sqrt{x_1^2+x_2^2}}\cos x_5-\sqrt{x_1^2+x_2^2}x_6\sin x_5 \tag{30}$$

$$\dot{x}_2=\frac{x_1x_3+x_2x_4}{\sqrt{x_1^2+x_2^2}}\sin x_5+\sqrt{x_1^2+x_2^2}x_6\cos x_5 \tag{31}$$

$$\dot{x}_5=x_6. \tag{32}$$

The state equation (20), the own-ship trajectory (30)–(32), and the measurement equation (21) are derived. The technique developed for estimation with *measurement likelihood* consists of a CKF and an OTE, as indicated in Fig. 3.

The preceding results are expressed in continuous form. Equation of state and measurement for discrete time may be deduced by assigning $t=kT$ where $k=1,2,\ldots$, and T denotes sampling period. Straightforward application of the discrete time Kalman filter to (20) and (21) yields the CKF algorithm as outlined below [15].

$\hat{\mathbf{D}}_{0/0}$: initial estimate of the CKF state vector.
$\mathbf{P}_{0/0}$: initial estimate of the CKF state vector error covariance matrix.

The CKF consists of the prediction process with

$$\hat{\mathbf{D}}_{k/k-1}=\Psi\hat{\mathbf{D}}_{k-1/k-1}+\mathbf{G}_T\mathbf{u}_{k-1} \tag{33}$$

$$\hat{\mathbf{D}}_{k/k}=\hat{\mathbf{D}}_{k/k-1}+\mathbf{K}_k(E_k-\mathbf{H}\hat{\mathbf{D}}_{k/k-1}) \tag{34}$$

where

$$\Psi=(I+\mathbf{F}T)\qquad \mathbf{G}_T=\mathbf{G}T\qquad \Gamma_T=\Gamma T.$$

The Kalman gain $\mathbf{K}_k$ is determined from the covariance term $\mathbf{P}_{k/k-1}$ of $\hat{\mathbf{D}}_{k/k-1}$ with

$$\mathbf{K}_k=\mathbf{P}_{k/k-1}\mathbf{H}^T(\mathbf{H}\mathbf{P}_{k/k-1}\mathbf{H}^T+R_v)^{-1} \tag{35}$$

$$\mathbf{P}_{k/k-1}=\Psi\mathbf{P}_{k-1/k-1}\Psi^T+\Gamma_TQ_v\Gamma_T^T \tag{36}$$

$$\mathbf{P}_{k/k}=(\mathbf{I}-\mathbf{K}_k\mathbf{H})\mathbf{P}_{k/k-1} \tag{37}$$

where Q_v and R_v represent the covariance of $\mathbf{W}$ and ε, respectively.

In deriving the OTE, consideration is first made of (30) and (31) when the CKF state $\hat{\mathbf{D}}_{k/k}$ at time k

becomes available

$$\hat{v}_x(k/k) = \frac{\hat{x}_1(k/k)\hat{x}_3(k/k) + \hat{x}_2(k/k)\hat{x}_4(k/k)}{\sqrt{\hat{x}_1^2(k/k) + \hat{x}_2^2(k/k)}} \sin x_5(k/k) - \sqrt{\hat{x}_1^2(k/k) + \hat{x}_2^2(k/k)}\hat{x}_6(k/k)\cos x_5(k/k) \tag{38}$$

$$\hat{v}_y(k/k) = \frac{\hat{x}_1(k/k)\hat{x}_3(k/k) + \hat{x}_2(k/k)\hat{x}_4(k/k)}{\sqrt{\hat{x}_1^2(k/k) + \hat{x}_2^2(k/k)}} \cos x_5(k/k) + \sqrt{\hat{x}_1^2(k/k) + \hat{x}_2^2(k/k)}\hat{x}_6(k/k)\sin x_5(k/k). \tag{39}$$

Equations (38) and (39) lead to $\mathbf{Z}_p(k+1)$ which can be defined as *measurement likelihood* by

$$\mathbf{Z}_p(k+1) = \mathbf{B}(k+1)\hat{\mathbf{Z}}_p(k) + \mathbf{n}_p(k+1) \tag{40}$$

where

$$\mathbf{B}(k+1) = \begin{bmatrix} 1 & 0 \\ 0 & 1 \end{bmatrix} \tag{41}$$

$$\mathbf{Z}_p(k+1) = [Z_{p1}(k+1) \quad Z_{p2}(k+1)]^T \tag{42}$$

$$\hat{\mathbf{Z}}_p(k) = [\hat{Z}_{p1}(k) \quad \hat{Z}_{p2}(k)]^T = [\hat{v}_x(k/k) \quad \hat{v}_y(k/k)]^T \tag{43}$$

and $\mathbf{n}_p(k+1) = [n_{p1}(k+1) \;\; n_{p2}(k+1)]^T$ represents the random error which is assumed to be zero-mean Guassian white with variance $E[\mathbf{n}_p(k)\mathbf{n}_p^T(k)] = \mathbf{S}_p\delta_{kj}$. The matrix $\mathbf{S}_p$ is normally regarded as a weighting matrix.

The predicted velocity states in x and y axes are given by outputs of the CKF as follows

$$\hat{\mathbf{r}}_e(k+1/k) = \mathbf{B}(k+1)\hat{\mathbf{r}}_e(k/k) \tag{44}$$

where

$$\hat{\mathbf{r}}_e(k/k) = [\hat{r}_{e1}(k/k) \quad \hat{r}_{e2}(k/k)]^T = [\hat{v}_x(k/k) \quad \hat{v}_y(k/k)]^T. \tag{45}$$

The OTE algorithm based on recursive filter form [8] then becomes

$$\mathbf{K}_p(k+1) = \gamma^{-1}\mathbf{P}_p(k)\mathbf{B}^T(k+1) \times [\mathbf{B}(k+1)\gamma^{-1}\mathbf{P}_p(k)\mathbf{B}^T(k+1) + S_p]^{-1} \tag{46}$$

$$\mathbf{P}_p(k+1) = [\mathbf{I} - \mathbf{K}_p(k+1)\mathbf{B}(k+1)]\gamma^{-1}\mathbf{P}_p(k) \tag{47}$$

$$\hat{\mathbf{r}}_e(k+1/k+1) = \hat{\mathbf{r}}_e(k+1/k) + \mathbf{K}_p(k+1) \times [\mathbf{Z}_p(k+1) - \mathbf{B}(k+1)\hat{\mathbf{r}}_e(k/k)] \tag{48}$$

where $\mathbf{K}_p(k+1)$ denotes gain matrix and $\mathbf{P}_p(k+1)$ is the error covariance of $\hat{\mathbf{r}}_e(k+1/k+1)$ which is treated as the input vector of the CKF in the next computational cycle. The operation of the estimator is pivoted about the values of the gain $\mathbf{K}_p(k+1)$,

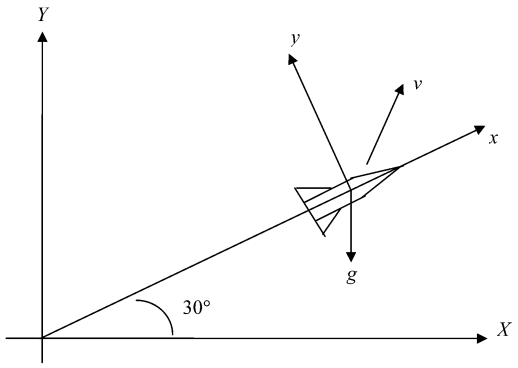

Fig. 4. Flight path of vehicle.

as shown in (48). The estimator "believes" the predicted estimate $\hat{\mathbf{r}}_e(k+1/k)$, which is obtained from output of the CKF for small $\mathbf{K}_p(k+1)$. The estimator believes the prediction error or innovation a function primarily of the *measurement likelihood* otherwise. A fading memory factor γ, $0 < \gamma \leq 1$, is used in this algorithm. The above algorithm reduces to that of usual sequential form when $\gamma = 1$. The correction gain $\mathbf{K}_p(k+1)$ for updating $\hat{\mathbf{r}}_e(k+1/k+1)$ in (48) is diminishing as k increases in this case, thereby allowing $\hat{\mathbf{r}}_e(k+1/k+1)$ to converge to the true value. However, $\mathbf{K}_p(k+1)$ should be prevented from reducing to zero in some practical applications. This is accomplished by introducing the factor γ. For $0 < \gamma < 1$, $\mathbf{K}_p(k+1)$ has effectively prevented it from shrinking to zero. Hence, the corresponding algorithm can continuously preserve its updating ability. The inherent data truncation effect brought on by γ, nevertheless, causes increased variances in $\hat{\mathbf{r}}_e(k+1/k+1)$ resulting from noise. A compromise must be made between fast adaptive capability and the loss of estimate accuracy.

IV. SIMULATION ANALYSIS

This section simulates a simple flight of a vehicle in 2 degrees of freedom (DOF). The simulation illustrates whether gravity can effectively bound the excursion of θ and $\mathbf{V}$. Fig. 4 reveals a straight flight with a vehicle body pitch angle of 30°. The acceleration along the vehicular x-axis is $2g$, the accelerometer bias is 10 mili-g, the initial conditions in position and velocity are $x(0) = 10$ m, $y(0) = 5$ m, $v_x(0) = 2$ m/s, and $v_y(0) = 2$ m/s. Moreover, assume that $\mathbf{W}$ and ε are all Gaussian distribution, the covariance are $\mathbf{Q}_v = (0.01)\mathbf{I}_{(3\times3)}T$ and $\mathbf{R}_v = (0.01)\mathbf{I}_{(6\times6)}/T$, respectively. The proposed algorithm is compared to the CKF algorithm without OTE for the test scenario. The following example indicates that the *measurements likelihood* in velocity can help determine the states in which the estimation promises a convergent trend. Thus, a measurement in initial attitude is bound all states by using the own-ship estimator.

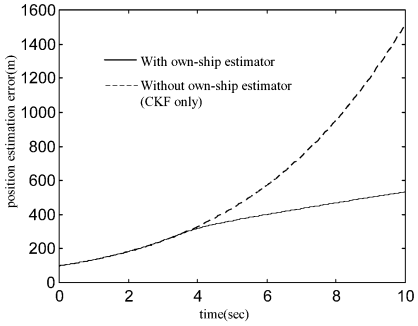

Fig. 5. Position estimation error in x axis.

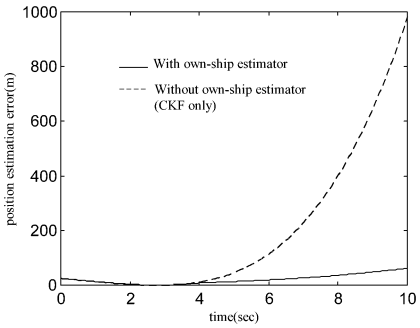

Fig. 6. Position estimation error in y axis.

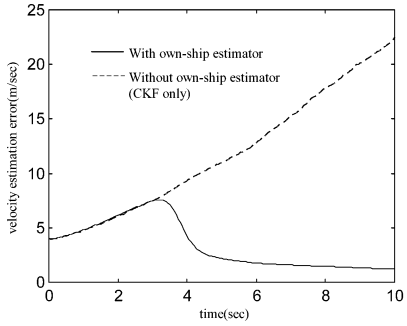

Fig. 7. Velocity estimation error in x axis.

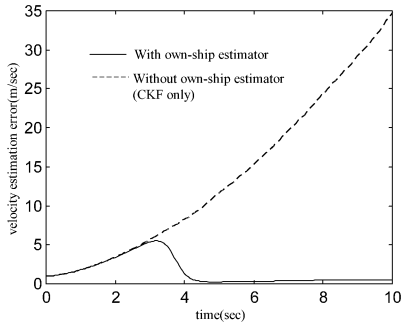

Fig. 8. Velocity estimation error in y axis.

Figs. 5–10 display the estimation errors of both the proposed method and the CKF. Figs. 5 and 6 present the errors of position in x and y, respectively, indicating that the CKF algorithm produces divergence and poor performance. Meanwhile the proposed algorithm presents good tracking accuracy. Figs. 7 and 8 compare the estimation errors between the CKF algorithm and the proposed algorithm in velocity. These figures obviously reveal that the estimation errors of the proposed algorithm rapidly converge within 5 s. Figs. 9 and 10 illustrate the estimation error in angle and angular rate, respectively, under a known initial attitude $G(\theta)$. It can obtain satisfactory angle and angular rate estimations both in CKF and the proposed algorithms. This example demonstrates that the CKF tracking algorithm yields poor estimation results for an unobservable system, and also suffers from the severely moderate convergence problem. It definitely requires the OTE filter to elevate the navigation accuracy.

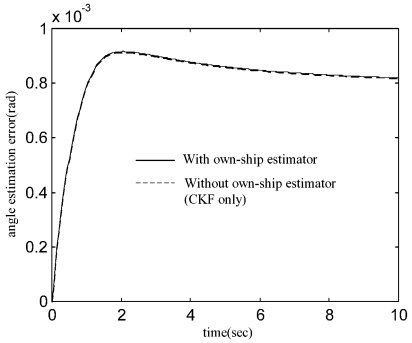

Fig. 9. Angle estimation error.

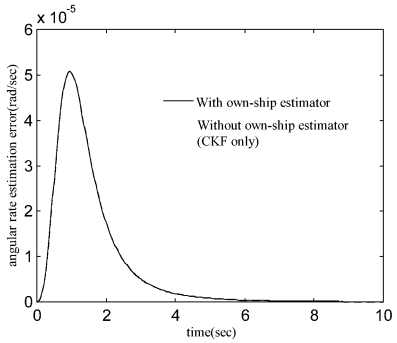

Fig. 10. Estimation error in angular rate.

V. CONCLUSIONS

This work presents a novel means of estimating. The six-accelerometer mechanization, with the state-of-the-art accelerometers, is highly promising in terms of its availability for short duration navigation. It also has the merits of low cost, rapid reaction, and high angular acceleration capability. Using the EEECE allows us to guarantee the stability. In addition, the presence of gravity in the accelerometers sensing give us a limit on initial attitude, thereby allowing it to sufficiently bound the angular velocity sign problem. Constructing a standard estimation form with *measurements likelihood* can be illustrated in detail by a planar motion. Any additional measurements on the dynamics state would help resolve this problem.

Performance could also be enhanced by deriving all possible sensor combinations. Since the proposed method is an acceleration type measurement unit. The interesting practical implementation of the proposed technique are MEMS of robot guidance, MAV, more accurate vibration monitoring device for industrial or biomechnical research.

APPENDIX A

Consider a states equation in general as

$$\dot{\mathbf{X}} = \mathbf{F}\mathbf{X} + \mathbf{G}\mathbf{u} + \Gamma\mathbf{W} \tag{49}$$

where $\mathbf{X}$, $\mathbf{u}$, and $\mathbf{W}$ stand for the states vector, the input vector, and the process noise respectively. $\mathbf{FX}$ represents the state transition term, $\mathbf{Gu}$ is the control, and $\Gamma\mathbf{W}$ is the disturbance. The measurement equation with measurement noise γ is

$$\mathbf{Y} = \mathbf{H}\mathbf{X} + \gamma. \tag{50}$$

Assume $\mathbf{W}$ and γ are two uncorrelated random variables.

The estimated states can be processed as below if the system is observable

$$\dot{\hat{\mathbf{X}}} = \mathbf{F}\hat{\mathbf{X}} + \mathbf{G}\mathbf{u} + \mathbf{K}(\mathbf{Y} - \hat{\mathbf{Y}}) \tag{51}$$

where $\hat{\mathbf{X}}$ means the estimated state, and $\hat{\mathbf{Y}}$ represents the predicted measurement. However, one of the measurements in all-accelerometer INS is acceleration which is the derivative of state. Two approaches are proposed for solving this problem. First, $\mathbf{H}$ matrix can be split into $\mathbf{H}_s$ and $\mathbf{H}_d$ corresponding to state vector and derivative of state respectively. Equation (50) can be reformulated as

$$\begin{aligned}\mathbf{Y} &= \mathbf{H}_s\mathbf{X} + \mathbf{H}_d\dot{\mathbf{X}} + \gamma \\ &= (\mathbf{H}_s + \mathbf{H}_d\mathbf{F})\mathbf{X} + \mathbf{H}_d\mathbf{G}\mathbf{u} + \mathbf{H}_d\Gamma\mathbf{W} + \gamma.\end{aligned} \tag{52}$$

The new measurement equation is a function of states only that have the same process as (50), however, it is not easy to treat in our problem. The second approach is to treat the highest derivative of state in measurement equation as a control input to eliminate the derivative term in measurement equation

$$y_d = \dot{x}_d + \gamma_d. \tag{53}$$

Then, we augment a new state equation

$$\dot{x}_d = y_d - \gamma_d. \tag{54}$$

We replace the equation x_d that are the highest derivatives with this kinematic equation.

Using the second solution regroup (49)–(51), and defining the estimation error

$$\tilde{\mathbf{X}} = \hat{\mathbf{X}} - \mathbf{X}. \tag{55}$$

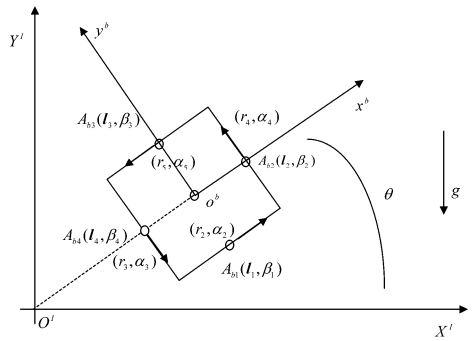

Fig. 11. Accelerometers in planar motion.

The estimation error equation is

$$\dot{\tilde{\mathbf{X}}} = (\mathbf{F} - \mathbf{K}\mathbf{H})\tilde{\mathbf{X}} - \mathbf{K}\gamma - \Gamma\mathbf{W}. \tag{56}$$

Equation (56) shows that the estimation error state has the characteristic equation EEECE as

$$\det(s\mathbf{I} - \mathbf{F} + \mathbf{K}\mathbf{H}) = 0. \tag{57}$$

It should avoid $s = 0$ roots.

APPENDIX B

We independently investigated the six-accelerometer configuration by a simple 2 DOF such as Fig. 11. The location and orientation of accelerometers in body frame are represented by $\mathbf{l}$ and $\boldsymbol{\beta}$, respectively, and the Euler angle of the vehicular with respect to the inertial frame is θ. To meet (11)–(14), we rearrange the sensing direction of accelerometers as

$$\begin{aligned}\mathbf{l} &= [\,l_1 \quad l_2 \quad l_3 \quad l_4\,] \\ &= \begin{bmatrix} 0 & 1 & 0 & -1 \\ -1 & 0 & 1 & 0 \end{bmatrix}\end{aligned} \tag{58}$$

$$\begin{aligned}\boldsymbol{\beta} &= [\,\beta_1 \quad \beta_2 \quad \beta_3 \quad \beta_4\,] \\ &= [\,\alpha_2\cos 45^\circ \quad \alpha_4\cos 135^\circ \quad \alpha_5\cos 45^\circ \quad \alpha_3\cos 135^\circ\,] \\ &= \begin{bmatrix} 1 & 0 & -1 & 0 \\ 0 & 1 & 0 & -1 \end{bmatrix}.\end{aligned} \tag{59}$$

The accelerometer output A_{oi}, $i = 1,2,3,4$ along each sensing direction, can be represented in compact form as

$$\begin{aligned}A_{oi} = \Bigg\{ &\begin{bmatrix} \cos\left(\theta + (i-1)\frac{\pi}{2}\right) & \sin\left(\theta + (i-1)\frac{\pi}{2}\right) \\ -\sin\left(\theta + (i-1)\frac{\pi}{2}\right) & \cos\left(\theta + (i-1)\frac{\pi}{2}\right) \end{bmatrix} \\ &\times \begin{bmatrix} \ddot{x} \\ \ddot{y} - \mathbf{g} \end{bmatrix} + \dot{\omega} \times \mathbf{r}_i + \omega_{i+1} \times (\omega_{i+2} \times \mathbf{r}_i) \Bigg\} \bullet \boldsymbol{\beta}.\end{aligned} \tag{60}$$

From (60), it can be combined to yield two sets of measurement representing rotational and linear accelerations at CG, respectively, as

$$y_{\dot{\omega}} = \tfrac{1}{4}(A_{o1} + A_{o2} + A_{o3} + A_{o4}) \tag{61}$$

and

$$y_a = \begin{bmatrix} y_{ax} \\ y_{ay} \end{bmatrix} = \begin{bmatrix} \dfrac{A_{o1} - A_{o3}}{2} \\ -\dfrac{(A_{o2} - A_{o4})}{2} \end{bmatrix}. \tag{62}$$

The state measurements in (61) and (62) do not have the unwanted ω^2 term but do have the gravity term. However, any additional measurements on $\mathbf{p}, \mathbf{V}, \theta, \omega$ can help some of the problem.

SOU-CHEN LEE
YU-CHAO HUANG
Department of System Engineering
Chung Cheng Institute of Technology
Tashi, Tao Yuan
Taiwan, 33509, R.O.C.

REFERENCES

[1] Bar-Itzhaxk, I. Y. (1993)
On two misconcepts in the theory of inertial navigation system.
AIAA93-3819-CP, 1993, 1067–1072.

[2] Schuler, A. R., et al. (1967)
Measuring rotational motion with linear accelerometer.
IEEE Transactions on Aerospace and Electronic Systems, **AES-3**, 3 (1967).

[3] Padgoankar, A. J., et al. (1957)
Measurement of angular acceleration of a rigid body using linear accelerometer.
Journal of Applied Mechanics (1957).

[4] Hu, A. S. (1977)
Rotational measurement of angular velocity without the use of gyro.
AIAA, 1977.

[5] DiNapoli, L. D. (1965)
The measurement of angular velocity without the use of gyro.
M.S. Thesis, The Moore School of Electric Engineering, University of Pennsylvania, Philadelphia, 1965.

[6] Algrain, M. C. (1991)
Accelerometer-based platform stabilization.
SPIE, **1482**, Acqusition, Tracking, and Pointing V (1991).

[7] Chen, J. H., Lee S. C., and Debra, D. B. (1994)
Gyroscope free strapdown inertial measurement unit by six linear accelerometers.
Journal of Guidance, Control and Dynamics, **17**, 2 (1994), 286–290.

[8] Franklin, G. F., Powell, J. D., and Workman, M. L. (1990)
Digital Control of Dynamic System (2nd ed.).
Reading, MA: Addison-Wesley, 1990.

[9] Aidela, V. J., and Hammel, S. E. (1983)
Utilization of modified polar coordinate for bearing-only tracking.
IEEE Transactions on Automatic Control, **AC-28**, 3 (1983), 283.

[10] Hammel, S. E., and Aidela, V. J. (1985)
Observability requirements for three-dimensional tracking via angle measurements.
IEEE Transactions on Aerospace and Electronic System, **AES-21**, 2 (1985), 200.

[11] Grossman, W. (1994)
Bearing-only tracking: A hybrid coordinate system approach.
Journal of Guidance, Control, and Dynamics, **17**, 3 (1994), 451.

[12] Stallard, D. V. (1987)
An angle-only tracking filter in modified spherical coordinates.
Presented at the AIAA Guidance, Navigation, and Control Conference, Monterey, CA, 1987.

[13] Greenwood, D. T. (1988)
Principles of Dynamics (2nd ed.).
Englewood Cliffs, NJ: Prentice-Hall, 1988.

[14] Siouris, G. M. (1993)
Aerospace Avionics Systems: A Modern Synthesis.
New York: Academic Press, 1993.

[15] Chui, C. K., and Chen, G. (1999)
Kalman Filtering with Real-Time Applications (3rd ed.).
New York: Springer-Verlag, 1999.

A Fuzzy Approach to Signal Integration

A new fuzzy concept for postdetection signal integration is presented. The fuzzy integrator is developed as a simple extension of the classic binary integrator by replacing the crisp binary threshold, which quantizes the observed data, with a fuzzy threshold. The performance of the fuzzy integrator is illustrated for detection of a simple nonfluctuating signal in Gaussian noise and is shown to exceed that of the binary integrator, approaching that of the optimal detector with Neyman–Pearson decision rule. Furthermore, the fuzzy integrator has the characteristic that the false alarm rate can be tuned using a single threshold, more easily than that of the dual-threshold binary integrator.

I. INTRODUCTION

Integration is a process used in signal detection by which data from multiple observations are combined to improve detection performance. There are two

Manuscript received October 29, 1999; revised February 27 and December 4, 2001; released for publication December 4, 2001.

IEEE Log No. T-AES/38/1/02602.

Refereeing of this contribution was handled by L. M. Kaplan.

This work was supported by Competitive Earmarked Research Grants (Hong Kong) 9040627 and 9040530.